

Single and vertically coupled type-II quantum dots in a perpendicular magnetic field: Exciton ground-state properties

K. L. Janssens,* B. Partoens,† and F. M. Peeters‡

Departement Natuurkunde, Universiteit Antwerpen (UIA), Universiteitsplein 1, B-2610 Antwerpen, Belgium

(Received 21 December 2001; revised manuscript received 5 April 2002; published 6 August 2002)

The properties of an exciton in a type-II quantum dot are studied under the influence of a perpendicular applied magnetic field. The dot is modeled by a quantum disk with radius R , thickness d and the electron is confined in the disk, whereas the hole is located in the barrier. The exciton energy and wave functions are calculated applying a self-consistent mean-field theory in the Hartree approximation using a finite difference mesh method. We distinguish two different regimes, namely, $d \ll 2R$ (the hole is located above and below the disk) and $d \gg 2R$ (the hole is located at the radial boundary of the disk), for which angular momentum (l) transitions are predicted with increasing magnetic field. We also considered a system of two vertically coupled dots where now an extra parameter is introduced, namely, the interdot distance d_z . For a sufficient large magnetic field, each l_h state becomes *spontaneous symmetry broken* with the electron and the hole moving towards one of the dots. This transition is induced by the Coulomb interaction and leads to a *magnetic-field-induced dipole moment*. No such symmetry-broken ground states are found for a single dot (and for three vertically coupled symmetric quantum disks). For a system of two vertically coupled truncated cones, which is asymmetric from the start, we still find angular momentum transitions. For a symmetric system of three vertically coupled quantum disks, the system resembles for small d_z the pillarlike regime of a single dot, where the hole tends to stay at the radial boundary, which induces angular momentum transitions with increasing magnetic field. For larger d_z the hole can sit between the disks and the $l_h=0$ state remains the ground state for the whole B region.

DOI: 10.1103/PhysRevB.66.075314

PACS number(s): 73.21.La, 71.35.Ji, 85.35.Be

I. INTRODUCTION

The study of self-assembled quantum dots,¹ as realized by the Stranski-Krastanow growth mode, has been a fascinating research area during the last decade. The possibility to discover new physics in these zero-dimensional structures together with possible applications in optoelectronics has led to many experimental and theoretical results. Most studies were devoted to type-I quantum dots,²⁻⁹ where both electron and hole are spatially located inside the quantum dots. Relatively few works, however, were done for type-II quantum dots, where electrons and holes are spatially separated. One expects from this type of dots interesting properties, such as large tunability of the emission energy and radiative lifetimes that are considerably longer than for their type-I counterparts.¹⁰

Within the group of type-II quantum dots, one can still distinguish between two systems. Namely, the system that confines the electrons inside the quantum dot, and forms an antidot for the hole, like, e.g., the InP/GaInP dots (if strain is neglected). Besides this, there are the systems, such as GaSb/GaAs (Ref. 11) and InAs/Si,¹² where the holes are confined within the dot, but where the electrons are located outside. Experimental studies on this type of quantum dots have been performed in Refs. 13-15 for the InP/GaInP system and in Refs. 11,16 for the GaSb/GaAs system. Theoretical investigations on InP/GaInP type-II dots were performed by Pryor *et al.*¹⁷ and Tadic *et al.*,¹⁸ who used a strain-dependent $\mathbf{k} \cdot \mathbf{p}$ Hamiltonian to calculate the electronic structure. Nomura *et al.*¹⁹ calculated the Landau levels in a high magnetic

field, solving the Hartree equations self-consistently, while the present authors studied an exciton in a planar quantum dot using a self-consistent mean-field theory in the Hartree approximation.²⁰ Lelong *et al.*²¹ calculated the binding energy of excitons, charged excitons, and biexcitons in GaSb/GaAs dots using the Hartree-Fock (HF) approximation. The magnetoexciton in a flat GaSb/GaAs dot was investigated by Kalameitsev *et al.*²² Strain effects are very important when studying self-assembled quantum dots: in Ref. 18 it was shown (in the absence of a magnetic field) that strain can invert the hole confinement potential in InP quantum dots, confining the hole inside the dot. Experimental results by M. Hayne *et al.*,¹⁴ however, led to the conclusion that the hole can also be located in the barrier material for InP quantum dots. The aim of the present study is to use a model as simple as possible to investigate the latter system. It is not our intention to obtain exact quantitative results, describing the real system, but to explore qualitatively the physics that is present in single and vertically coupled type-II systems.

In the present paper we study a single electron-hole pair bound by the Coulomb interaction, i.e., an exciton, in a *model* type-II quantum dot. The quantum dot is modeled by a quantum disk of finite height, which is an extension of our previous work²⁰ where we did not take into account the z direction. As an example, we consider the electron in the dot and the hole in the barrier material. The conclusions of our paper are also valid for the reverse situation where the hole is inside the dot and the electron is outside the dot. In the present work, we neglect strain effects and for the confinement potential we use a hard wall of finite height, confining

the electron inside the dot and repelling the hole to the barrier region. Furthermore, a magnetic field was applied in the growth direction, i.e., $\mathbf{B} = B\mathbf{e}_z$.

The first part of this paper deals with the study of the exciton in a single dot. Investigation of the influence of the disk parameters, namely, the radius R and thickness d , showed that one can distinguish between two regimes: the disklike regime and the pillarlike regime. For the first one, the disk thickness d is much smaller than its diameter, i.e., $d \ll 2R$, whereas the latter one describes the system with $d \gg 2R$. Although the magnetic field couples only with the in-plane electron and hole coordinates, we will show that these systems, with different z extension, behave very differently under an applied magnetic field.

In the second part of the paper, we study the properties of vertically coupled quantum dots. The interest of this study lies in the following. It is generally known that in reality self-assembled quantum dots resemble more our disklike system than our pillarlike system. However, it is also known that it is not too difficult to form vertical stacks of these disklike dots and thereby create a system that could behave like a pillarlike system.

The paper is organized as follows. In Sec. II, we give a brief discussion of our theoretical model. The numerical results in the absence of a magnetic field are presented in Sec. III. Section IV deals with the result for a perpendicular applied magnetic field. Section IV A discusses the results for the single dot disklike system, whereas Sec. IV B is dedicated to the pillarlike system. Sections IV C and IV D deal with two vertically coupled dots, respectively, disks and truncated cones. Sections IV E and IV F deal with three vertically coupled dots, respectively, for small and large interdot distances. Finally, we make a small revision of the results for the single disk in Sec. IV G. Our results are summarized in Sec. V.

II. THEORETICAL MODEL

We extended our previous approach,²⁰ which was valid for planar dots, and include the z direction. The energies and wave functions are solved within the effective-mass approximation (with m_e and m_h the effective electron and hole masses, respectively, $r_{e,h} = \sqrt{x_{e,h}^2 + y_{e,h}^2}$, $\omega_{c,e} = eB/m_e$ and $\omega_{c,h} = eB/m_h$) and the single-particle equations can be written as

$$\left[-\frac{\hbar^2}{2m_e} \frac{1}{r_e} \frac{\partial}{\partial r_e} \left(r_e \frac{\partial}{\partial r_e} \right) - \frac{\hbar^2}{2m_e} \frac{\partial^2}{\partial z_e^2} + \frac{\hbar^2}{2m_e} \frac{l_e^2}{r_e^2} + \frac{l_e}{2} \hbar \omega_{c,e} \right. \\ \left. + \frac{1}{8} m_e \omega_{c,e}^2 r_e^2 + V_e(r_e, z_e) \right. \\ \left. - \frac{e^2}{4\pi\epsilon} \int \frac{\rho_h(r', z')}{|\mathbf{r} - \mathbf{r}'|} d\mathbf{r}' \right] \psi_e(r_e, z_e) = \epsilon_e \psi_e(r_e, z_e), \quad (1a)$$

$$\left[-\frac{\hbar^2}{2m_h} \frac{1}{r_h} \frac{\partial}{\partial r_h} \left(r_h \frac{\partial}{\partial r_h} \right) - \frac{\hbar^2}{2m_h} \frac{\partial^2}{\partial z_h^2} + \frac{\hbar^2}{2m_h} \frac{l_h^2}{r_h^2} - \frac{l_h}{2} \hbar \omega_{c,h} \right. \\ \left. + \frac{1}{8} m_h \omega_{c,h}^2 r_h^2 + V_h(r_h, z_h) \right. \\ \left. - \frac{e^2}{4\pi\epsilon} \int \frac{\rho_e(r', z')}{|\mathbf{r} - \mathbf{r}'|} d\mathbf{r}' \right] \psi_h(r_h, z_h) = \epsilon_h \psi_h(r_h, z_h), \quad (1b)$$

where we made use of the axial symmetry by taking $\Psi_e(r_e, \varphi_e, z_e) = e^{il_e\varphi_e} \psi_e(r_e, z_e)$ and $\Psi_h(r_h, \varphi_h, z_h) = e^{il_h\varphi_h} \psi_h(r_h, z_h)$, and where the densities $\rho_e(r', z')$ and $\rho_h(r', z')$ are given by, respectively, $|\Psi_e(r_e, \varphi_e, z_e)|^2$ and $|\Psi_h(r_h, \varphi_h, z_h)|^2$. We made use of a finite difference scheme to solve the equations. More details about the implementation of this finite difference scheme can be found in Refs. 23,20. Note that we consider only a single electron and single hole and therefore there are no exchange terms. As confinement potentials we take hard walls of finite height,

$$V_{e,h}(r_e, z_e, r_h, z_h) = \begin{cases} V_{e,h} & r_{e,h} > R \quad \text{and} \quad |z_{e,h}| > d/2 \\ 0 & \text{otherwise,} \end{cases} \quad (2)$$

with R the radius of the disk, and where we took V_e positive and V_h negative. Note that the only good quantum number is the total angular momentum in the z direction, defined by $L = l_e + l_h$.

We solved the equations self-consistently using an iterative procedure. Since only the electron is confined in the absence of any Coulomb interaction, we start with the free-electron solution. The Hartree integrals are then integrated numerically as

$$\int \frac{\rho(r', z')}{|\mathbf{r} - \mathbf{r}'|} d\mathbf{r}' = 4 \int dz' \int dr' \frac{\rho(r', z') r'}{\sqrt{(r+r')^2 + (z-z')^2}} \\ \times \mathcal{K} \left(\frac{4rr'}{(r+r')^2 + (z-z')^2} \right), \quad (3)$$

where $\mathcal{K}(x)$ is the complete elliptic integral of the first kind. More details about the calculation and numerical implementation of this integral is given in Ref. 20.

After convergence of the iteration procedure, the total energy is given by

$$E_{\text{exciton}} = \epsilon_e + \epsilon_h + \frac{e^2}{4\pi\epsilon} \int \int \frac{\rho_e(r, z) \rho_h(r', z')}{|\mathbf{r} - \mathbf{r}'|} d\mathbf{r} d\mathbf{r}'. \quad (4)$$

The contribution of the correlation to the total energy is neglected in HF, but for the self-assembled quantum dots, it is expected to be less than 2% (Ref. 5) and for type-II dots this will be even less.

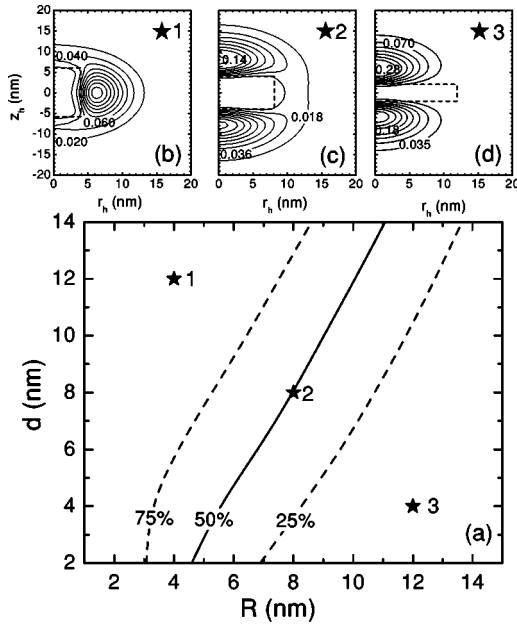


FIG. 1. (a) Phase diagram of the probability for the hole wave function to sit at the radial border of the disk, as a function of both R and d . (b), (c), and (d) are contour plots of the hole wave function, at the positions as indicated by the corresponding numbers on the main figure. The dashed lines in the contour plots indicate the boundary of the disk.

III. NUMERICAL RESULTS IN THE ABSENCE OF AN APPLIED MAGNETIC FIELD

In our model system, there are two main parameters that can be varied: the radius of the disk R , and the thickness of the disk d . In the first part of our numerical study we will investigate the influence of these parameters on the exciton energy and wave function in the absence of a magnetic field. Following material parameters, typical for the InP/InGaP dot system, were taken: $m_e = 0.077m_0$, $m_h = 0.60m_0$, $\epsilon = 12.61$, $V_e = 250$ meV, and $V_h = -50$ meV.

The variation of the disk radius R and thickness d has large consequences for the hole wave function. Namely, the hole always tends to sit as closely as possible to the electron. In this way, when the disk thickness is larger than its diameter ($d \geq 2R$), the hole will prefer to sit at the radial boundary of the disk. When we consider very thin disks, however, ($d \leq 2R$), it will be much more favorable for the hole to be located above and below the disk. This state was not possible in our previous study²⁰ of the two-dimensional flat quantum dot, where the hole was forced to sit at the radial boundary of the dot. To illustrate this, we calculated the probability to find the hole at the radial boundary of the disk as

$$P_{side} = 2\pi \int_{-\infty}^{\infty} dz_h \int_R^{\infty} dr_h r_h |\Psi_h(r_h, z_h)|^2. \quad (5)$$

When calculating this value for varying R and d , we obtained a phase diagram for the position of the hole wave function, which is shown in Fig. 1(a). The hole confinement potential in all these calculations was fixed to $V_h = -50$ meV. The solid curve indicates where 50% of the hole is located at the

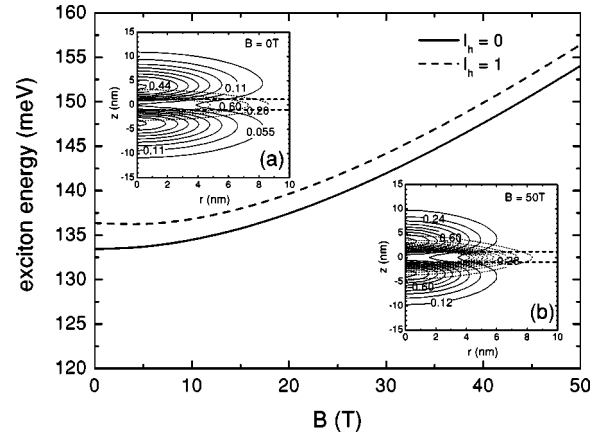


FIG. 2. The variation of the exciton energy with increasing magnetic field, for a disk with thickness $d = 2$ nm and radius $R = 10$ nm and two values of the hole angular momentum. The insets show the electron (dashed curve) and hole (solid curve) wave function for (a) $B = 0$ T and (b) $B = 50$ T.

radial boundary, for the dashed curves it is, respectively 25% and 75%. In order to have a more visual picture of the hole state, we present contour plots of the hole wave function $|\Psi_h(r_h, z_h)|^2$ for three characteristic situations in the phase diagram, as indicated by the numbered stars. Figure 1(b) shows the hole density for $R = 4$ nm, $d = 12$ nm, where the dotted lines indicate the boundary of the quantum disk. We clearly see that the hole is mainly situated at the radial side of the disk. Figure 1(c) was made for $R = 8$ nm, $d = 8$ nm and at this position, exactly 50% of the wave function is located at $r_h > R$. The third plot, Fig. 1(d), depicts the result for a thin disk, with $R = 12$ nm and $d = 4$ nm, where the hole wave function is mostly located above and below the disk, where it is nearer to the electron.

Thus we can distinguish between two main systems: (a) a disklike system with $d \leq 2R$, where the hole will be located above or below the quantum disk, and (b) a pillarlike system with $d \geq 2R$, where the hole sits mainly at the radial boundary of the disk. The solid line in Fig. 1(a) can be approximated by the curve $d = 1.76R - 5.41$ nm. We will see in the following section that a magnetic field has a very different effect on these two classes of systems.

IV. RESULTS FOR A PERPENDICULAR APPLIED MAGNETIC FIELD

A. Single dot: A disklike system

After having discussed the influence of the main parameters of our system, we are now ready to consider an extra feature, i.e., a magnetic field applied along the z direction, parallel to the growth direction. The magnetic field will squeeze the wave functions in the radial direction. When $d \leq 2R$, the hole is above and below the disk, and will be pressed stronger to the center of the disk. Figure 2 depicts the exciton energy as a function of the magnetic field for a disk with $R = 10$ nm and $d = 2$ nm for two different values of the hole angular momentum l_h . Note that this exciton energy includes both the one-particle energies and the Coulomb en-

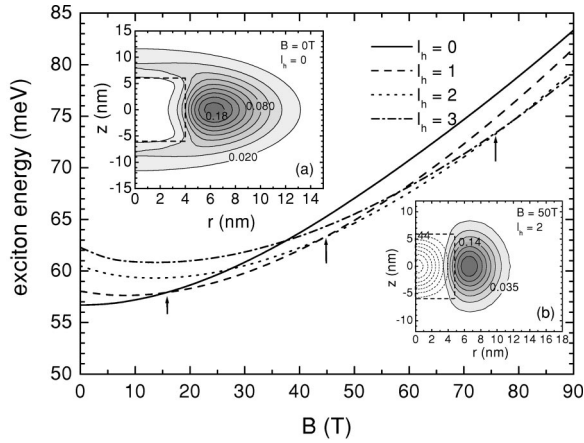


FIG. 3. Evolution of the exciton energy with increasing magnetic field, for a disk with thickness $d=12$ nm and radius $R=4$ nm. Increasing the magnetic field, leads to successive transitions of the hole angular momentum l_h indicated by the arrows. The insets depict contour plots of the electron (dashed contour lines) and hole wave functions at $B=0$ T (a), and $B=50$ T (b). The dashed line indicates the disk boundary.

ergy, i.e., $E_{exciton} = E_e + E_h - E_{coul}$. In the present case the single hole energy E_h will be 0, as the single hole is not confined. The single electron energies at $B=0$ T and $B=50$ T are given by, respectively, $E_e = 192.6$ meV and $E_e = 212.3$ meV. We find a strong enhancement of the exciton energy of almost 20 meV for $B=0$ T \rightarrow $B=50$ T. Due to the magnetic field, the electron and hole are both pushed closer to the center, which enhances the Coulomb interaction. However, also the one-particle electron energy increases drastically with increasing magnetic field, thus canceling the effect of the enhanced (negative) Coulomb energy. The two insets show what happens with the electron (dashed curves) and hole (full curves) wave functions when a magnetic field is applied. For $B=0$ T [Fig. 2(a)] the electron is strongly confined in the quantum disk, and the hole is localized above and below the disk. From the figure, it is obvious that this position is energetically most favorable for the hole, since the hole will be very close to the electron. Because of the very small thickness, there is some smearing of the electron wave function out of the disk in the z direction, which attracts the hole to this position. The corresponding wave functions for $B=50$ T are plotted in Fig. 2(b), where again the dashed curve indicates the electron wave function, and the solid curve the hole. We see that both particles are compressed in the radial direction. For the electron, this leads to a further penetration of the wave function into the barrier. Because of this, the hole will be even stronger attracted to the top and bottom of the disk, which leads to a larger penetration of the hole in the disk. As a result, the hole wave function will also be slightly squeezed in the z direction.

B. Single dot: A pillarlike system

The exciton energy as a function of the magnetic field is plotted in Fig. 3 for the case of $R=4$ nm, $d=12$ nm, and $V_h = -50$ meV. An interesting feature that appears is the oc-

currence of (hole) angular momentum transitions with increasing magnetic field. The origin of the angular momentum transitions is the following. As discussed in Sec. III, the preferred position of the hole for a disk with a thickness larger than its diameter will be at the radial boundary of the disk. When a magnetic field is applied along the z direction, the hole will be pushed against the border of the disk. Since the disk forms a barrier for the hole, it will be energetically more favorable to jump to a higher angular momentum l_h state. Notice that l_h is an approximate quantum number. This feature was also apparent in our previous study of planar type-II dots,²⁰ where we forced the hole to sit at the radial boundary. This is similar to an exciton in a quantum-ring structure.^{24,25}

In the present study, however, we allow for the hole to relax also in the z direction. Therefore, for a small thickness of the disk (disklike system), it will be much more favorable for the hole to move in the z direction and only for thick enough disks, such l_h transitions occur. Contour plots of the wave functions are shown, respectively, for the hole at $B=0$ T [Fig. 3(a)] and at $B=50$ T [Fig. 3(b)] and for the electron at $B=50$ T [Figs. 3(b), dashed contour lines]. We find that the electron is located in the center of the disk, with almost no penetration into the barrier. At $B=0$ T, the hole is mainly sitting at the radial boundary of the disk, although there is some extent of the wave function towards the top and bottom of the disk, and there is also some penetration into the dot. When increasing the magnetic field, the hole jumps to the $l_h=1$ state around $B \approx 15$ T. When an angular momentum transition occurs, the hole is pushed at the side, where it has more space to extend in the radial direction. Further increasing the magnetic field leads to a jump to $l_h=2$ at $B \approx 45$ T and to $l_h=3$ at $B \approx 79$ T. In the absence of those l_h transitions, the magnetic field would have compressed the hole much more strongly to the radial boundary of the disk, which leads to a larger energy as is shown clearly by the solid curve in Fig. 3.

In order to investigate the influence of the hole confinement potential V_h on the angular momentum transitions, we made a phase diagram of the angular momentum state of the hole as a function of both the confinement potential and the magnetic field. This is shown in Fig. 4 for a disk with radius $R=6$ nm and thickness $d=14$ nm. The figure shows that up to $V_h = -13$ meV no angular momentum transitions occur. In this region V_h is too small to form a barrier for the hole, and the hole jumps inside the disk due to the Coulomb interaction, forming a type-I system. We also see that the transition between type-I and type II is very sharp. In our previous study of the planar dots,²⁰ we found from a similar figure a reentrant behavior to the $l_h=0$ state for sufficient large magnetic fields. This is not so evident in the present case, as we find that the line that separates the type-I from the type-II behavior is almost vertical.

From an experimental point of view, it is interesting to look at the probability for recombination of the exciton, which is proportional to the square of the overlap integral

$$I = \int \Psi_e(\mathbf{r}) \Psi_h(\mathbf{r}) d\mathbf{r} = \int_0^{2\pi} e^{i(l_e + l_h)\varphi} d\varphi \int_0^\infty \psi_e(r) \psi_h(r) r dr. \quad (6)$$

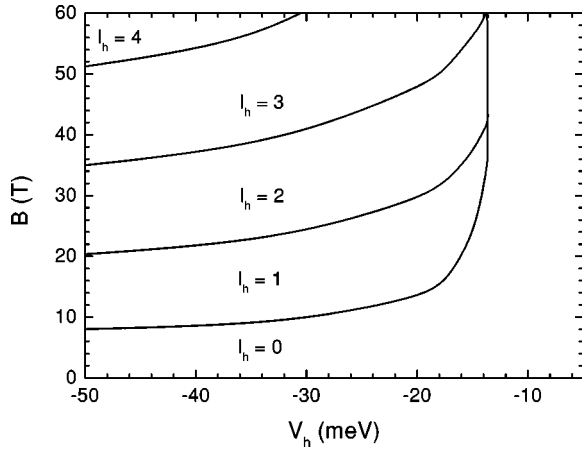


FIG. 4. Phase diagram of the angular momentum transitions as a function of the hole confinement potential V_h and the magnetic field B , for a disk radius $R=6$ nm and thickness $d=14$ nm.

The integral over the angle gives $2\pi\delta_{l_e+l_h}$. This means that the probability for deexcitation is only nonzero for $l_e+l_h=0$. This implies that, after an angular momentum transition, the probability for recombination decreases strongly, leading to a vanishing of the photoluminescence spectrum after a certain value of the magnetic field. Figure 5 depicts the overlap integral I as a function of the magnetic field, for $V_h=-10$ meV (solid curve) and $V_h=-30$ meV (dashed curve). For $V_h=-10$ meV the system is type I, as was demonstrated in the preceding paragraph, and therefore the ground state will always be the $l_h=0$ state, and the overlap integral is always nonzero. However, as the system transits from type I to type II we see a strong decrease of the overlap, because the exciton becomes spatially indirect. Also for $V_h=-30$ meV, we find a different behavior as function of the magnetic field: after the system has jumped to a higher angular momentum state, the overlap integral becomes zero. This is due to the fact that the condition $l_e+l_h=0$ is no

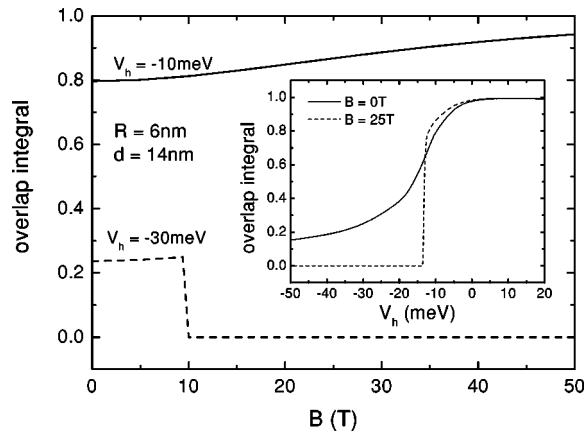


FIG. 5. Overlap integral as a function of the magnetic field for two values of the confinement potential of the hole $V_h=-10$ meV (solid curve) and $V_h=-30$ meV (dashed curve). The overlap integral as function of the hole confinement potential is shown in the inset for $B=0$ T (solid curve) and $B=25$ T (dashed curve).

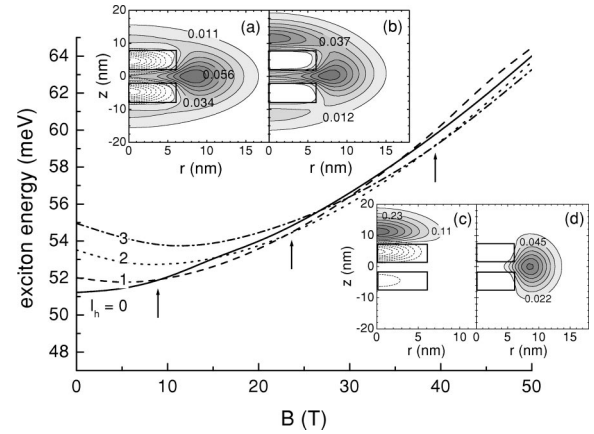


FIG. 6. Exciton energy as function of the magnetic field, for two coupled disks with $R=6$ nm, $d=6$ nm, and $d_z=3.6$ nm. The insets show contour plots of the wave functions for $l_h=0$ at, respectively, $B=0$ T (a), $B=15$ T (b), and $B=30$ T (c) (electron: dashed contour lines), and for $l_h=3$ at $B=50$ T (d).

longer fulfilled. The inset shows the evolution of the overlap integral with the confinement potential of the hole. For $B=0$ T, the ground state of the system is always $l_h=0$ and therefore the overlap is nonzero. For $B=25$ T, we can derive from this figure also the transition from type-I to type II: for a type-I system, there are no angular momentum transitions and the overlap integral has a finite value. For a type-II system, however, angular momentum transitions occur, and the overlap becomes zero.

C. Two vertically coupled dots

The inclusion of the z direction in our calculation enables us to investigate systems of vertically coupled quantum dots. We have now an extra parameter to vary, namely, the interdot distance d_z . In this first part, we focus on two stacked dots of the same size, namely radius $R=6$ nm and thickness $d=6$ nm, and with $d_z=3.6$ nm. The total stack height of 15.6 nm is thus larger than the diameter of the disks, being 12 nm. Therefore we expect to find a magnetic-field behavior which resembles that of the single-disk pillarlike system. The result for the exciton energy as function of the magnetic field is shown in Fig. 6. Indeed we find angular momentum transitions with increasing magnetic field. Figure 6(a) depicts contour plots of the electron (dashed contour lines) and hole wave functions at $B=0$ T and shows that the electron is symmetrically distributed over the two disks. The Coulomb interaction attracts the hole as close as possible to the electron, in this case the radial boundary of the disks. As one can see, the hole tends also to sit between the disks, to be even closer to the electron. A magnetic field acts on the wave functions in the radial direction, and thereby pushes the hole stronger between the disks. There is, however, not enough space, and therefore it will be energetically more favorable for the hole to jump to a higher l_h state.

When giving a closer look at the behavior of the different l_h states in a magnetic field (Fig. 6), a remarkable feature appears: the $l_h=0$ curve exhibits a kind of kink around $B=15$ T, and we find a similar feature for $l_h=1$ around B

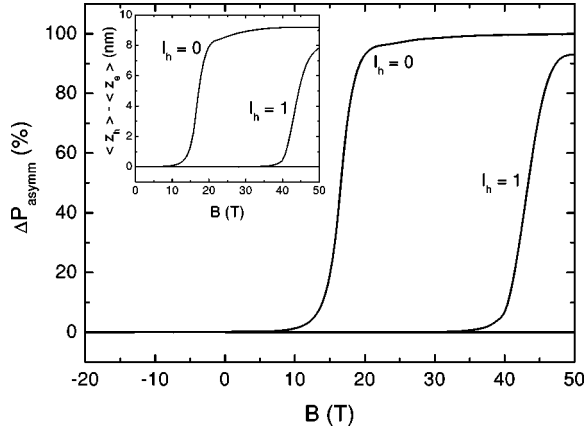


FIG. 7. Degree of asymmetry of the different l_h states as a function of the magnetic field. The inset shows the dipole moment as a function of the magnetic field.

=45 T. Investigation of the wave functions [Figs. 6(b,c)] tells us that we are dealing with a *spontaneous symmetry breaking*.²⁶ The corresponding hole wave function at $B = 15$ T and 30 T, for $l_h = 0$, is shown in Fig. 6(b,c), respectively, where one can see clearly the increase of asymmetry with magnetic field. But for such magnetic fields the $l_h = 0$ state is not the ground state. This means that the jump to a higher angular momentum state is still preferred above the asymmetric state [see Fig. 6(d) for $l_h = 3$ and $B = 50$ T]. We also found that with increasing l_h the symmetry breaking will occur at larger magnetic fields.

In order to investigate whether or not the ground-state configuration is asymmetric, we calculated

$$\Delta P_{asymm} = 2\pi \int_0^\infty dr_h r_h \left(\int_0^\infty dz_h - \int_{-\infty}^0 dz_h \right) |\Psi_h(r_h, z_h)|^2, \quad (7)$$

which expresses the degree of asymmetry of the hole wave function in the z direction. This quantity is plotted in Fig. 7 as function of the magnetic field for $l_h = 0, 1, 2, 3$. This plot confirms that after $B \approx 15$ T the $l_h = 0$ state becomes highly asymmetric, and for higher B also $l_h = 1$ becomes asymmetric. The asymmetric states for the subsequent l_h states occur for $B > 50$ T. The contour plot of the hole wave function at $B = 50$ T is shown in Fig. 6(d) for the ground state, which is $l_h = 3$. The inset of Fig. 7 shows the dipole moment for the different l_h states with increasing magnetic field. This is an interesting quantity, as it can be measured experimentally. Note that for our symmetric system, we have the unique feature that a magnetic field is able to induce a dipole moment.

We can understand the spontaneous symmetry breaking as follows. In the asymmetric case the electron wave function is of course attracted to the hole [see Fig. 6(c), dashed lines] and thus stronger confined, in this way increasing its single-particle energy. Therefore, the broken-symmetry state can only occur if it can overcome this increase in energy due to a larger Coulomb attraction between electron and hole. We mentioned that an increasing magnetic field favored the

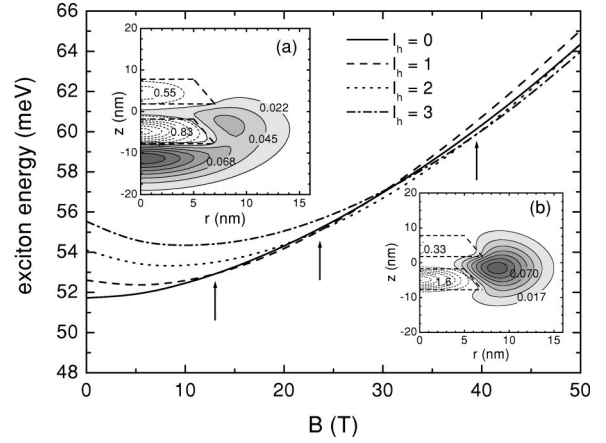


FIG. 8. Evolution of the exciton energy with the magnetic field for two coupled truncated cones. The insets show contour plots of the electron (dashed contour lines) and hole wave functions at $B = 0$ T (a) and at $B = 30$ T (b). The dashed lines indicate the disk boundary.

broken-symmetry state. The reason is that with increasing magnetic field the electron becomes stronger confined in the dot, and consequently expels more in the z direction. In the broken-symmetry case it even expels more, resulting in a larger overlap with the hole, which can eventually make the asymmetric state lower in energy than the symmetric state. If this is true, then the broken symmetry would occur even sooner with increasing magnetic field for thinner disks, where the electron is expelled more in the barrier material in the z direction. We found that this is indeed the case for two thin vertically coupled disks ($R = 12$ nm, $d = 3$ nm, and $d_z = 3$ nm, $l_h = 0$). For this system, we find already a broken-symmetry state for zero magnetic field. In this case, this broken-symmetry state is also the ground state.

D. Two vertically coupled truncated cones

It is now interesting to check whether the above angular momentum transitions survive in a system that is completely asymmetric from the beginning, such as a system of two vertically coupled truncated cones. The two cones are equal, and defined by a base radius R_b of 7 nm, a thickness $d = 6$ nm, and an angle of 71° (dashed lines in the insets of Fig. 8). The hole and electron wave function [Figs. 8(a), electron: dashed contour lines] show indeed the asymmetric behavior, at $B = 0$ T and for $l_h = 0$. The result for the exciton energy as a function of the magnetic field is depicted in Fig. 8. The interesting feature is that, even for this system, angular momentum transitions occur. Since there is still some part of the hole wave function located at the radial border and also some part between the disks, it appears to be still more favorable for the hole to jump to the higher l_h state than to move more and more below the disk. Figure 8(b) shows a contour plot of the hole wave function in the ground state for $l_h = 2$ at $B = 30$ T.

E. Three vertically coupled dots: Small interdot distance d_z

For simplicity we consider only the case of three identical dots. The first system under investigation contains three ver-

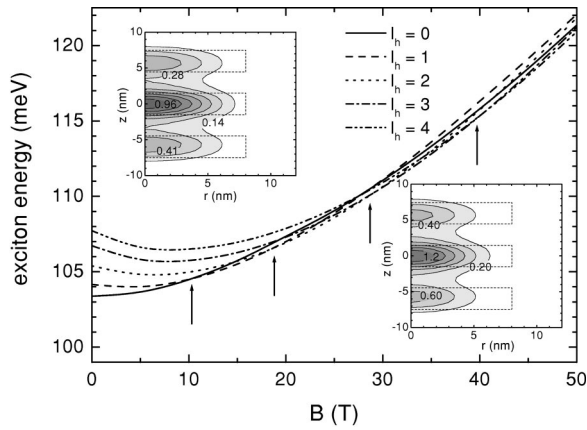


FIG. 9. Exciton energy as a function of the magnetic field for three vertically coupled disks ($R=8$ nm, $d=3$ nm) with interdot distance $d_z=3$ nm. Increasing the magnetic field leads to angular momentum transitions, which are indicated by the arrows. The insets show contour plots of the electron wave functions at, respectively (a) $B=0$ T and (b) $B=50$ T. The dashed lines indicate the disk boundaries.

tically coupled quantum disks, each with disk radius $R=8$ nm, disk thickness $d=3$ nm, and with interdot distance $d_z=3$ nm. In this case the confinement of the hole V_h was taken to be -30 meV. Figure 9 shows the result for the exciton energy as a function of the magnetic field. Similar to the case of the pillarlike single dot, we find angular momentum transitions with increasing magnetic field. The origin of these angular momentum transitions can be understood by looking at the wave functions. The insets of Fig. 9 show the electron wave functions at (a) $B=0$ T and (b) $B=50$ T, and it appears that the main part is located in the middle dot, whereas there is some small extent of the wave function into both the upper and lower dots. At $B=50$ T, the wave function is more squeezed in the radial direction. The evolution of the hole wave function with increasing magnetic field is depicted in Fig. 10. At $B=0$ T [Fig. 10(a)], the main part of the hole wave function is situated at the radial boundary of the stacked system and its probability to sit at the radial side is $P_{side}=73\%$. There is some extent of the wave function towards the top and bottom of the stack, and also between the dots. When the magnetic field increases [Fig. 10(b), $B=10$ T], the wave function is pushed further between the disks, because it prefers to sit as closely as possible to the electron. However, there is not enough space between the disks to confine the whole wave function, and therefore it is energetically more favorable for the hole to jump to a higher angular momentum state. Further increasing the magnetic field leads to more angular momentum transitions [Figs. 10(c-f)].

As can be seen from the wave functions, the ground state for this system is always symmetric. The asymmetry, as found in the two-disks system, is, however, still present, but it turns out not to be the ground state. For the $l_h=0$ state, the wave functions become asymmetric at about $B=20$ T, resulting in a slight bow in the full curve of Fig. 9. The fact that the asymmetry is less pronounced in this system can be understood as follows: in the three-disks system the main

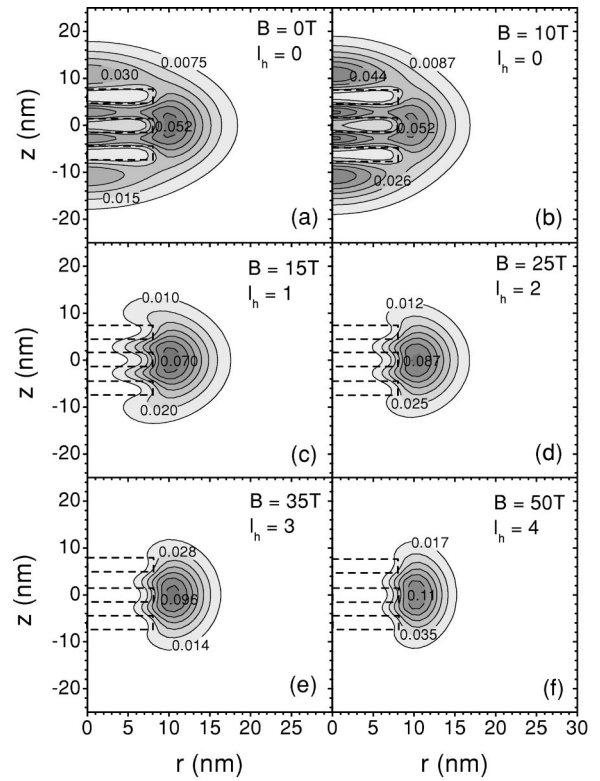


FIG. 10. Contour plots of the hole wave function corresponding to Fig. 9 for (a) $B=0$ T, (b) $B=10$ T, (c) $B=15$ T, (d) $B=25$ T, (e) $B=35$ T, and (f) $B=50$ T. The dashed lines indicate the disk boundaries.

part of the electron is located in the middle disk. This is in contrast to the two-disks system, where the electron wave function has equal parts located in the two disks. Even when an asymmetry is induced in the present three-disks system, the electron will still be mainly located in the middle disk, and therefore the hole will sit more tightly at the radial boundary than was the case for the two coupled disks.

F. Three vertically coupled dots: Large interdot distance d_z

When we increase the interdot distance d_z up to 5.5 nm, the hole will start to be confined between the disks. Figure 11 shows that there are no angular momentum transitions for this system and it resembles very much the narrow disklike system (see Fig. 2). In this figure the solid curve denotes the $l_h=0$ state, whereas the dashed curve denotes the $l_h=1$ curve. We turn again to the wave functions to explain this behavior. The electron is sitting mainly in the middle dot, this time with smaller extent into the upper and lower dots [Figs. 11(a) and 11(b) for, respectively, $B=0$ T and $B=50$ T, dashed contour lines]. The contour plot for the hole wave function [Fig. 11(a)] shows that already at $B=0$ T the hole is completely situated between the disks. This is the preferred place for the hole, as it tends to sit as close as possible to the electron. Further increasing the magnetic field squeezes the wave function more in the radial direction [Fig. 11(b)]. As there is still enough space between the disks, there

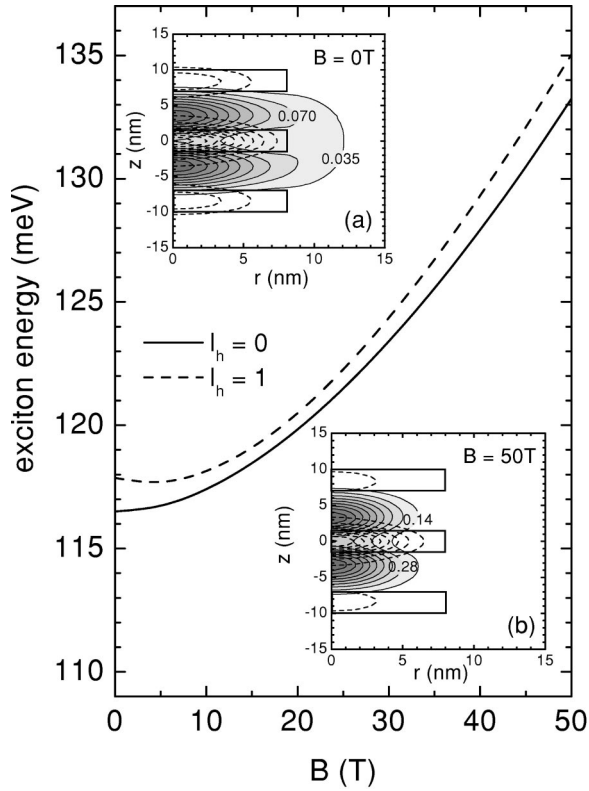


FIG. 11. Exciton energy as a function of the magnetic field, for three vertically coupled disks ($R=8$ nm, $d=3$ nm) with interdot distance $d_z=5.5$ nm. The insets are contour plots of the electron (dashed contour lines) and hole wave functions for (a) $B=0$ T and (b) $B=50$ T. The dashed lines indicate the disk boundaries.

is no need for the hole to jump to a higher angular momentum state, and $l_h=0$ remains the ground state over the whole B region.

For this case, no asymmetry occurs up to $B=50$ T. This means that this system is quite stable against spontaneous symmetry breaking. This stability is due to the fact that again the electron is strongly located in the middle disk, and that the hole is now sitting between the disks instead at the radial boundary.

G. Revision of the results for the single-disk systems

We now turn back to the single-disk systems, both the disklike and the pillarlike, where we did not talk about broken-symmetry solutions. However, also in this case they can be found.

We find that the disklike system, i.e., $R=10$ nm and $d=2$ nm, is perfectly stable up to $B=50$ T and we find no asymmetric behavior. This is in perfect agreement with the result for the three coupled disks with $d_z=5.5$ nm. Indeed, for the disklike system we have again the electron sitting in the disk with the hole above and below the disks, which is quite similar to the second three-disks system.

For the pillarlike system, i.e., $R=4$ nm and $d=12$ nm, we do find an asymmetry, but only for the $l_h=0$ state and at very high magnetic fields, i.e., starting around $B=80$ T. The difference in energy between the states with symmetric and

antisymmetric wave functions is only 0.08 meV for $B=90$ T. The ground state, however, remains symmetric over the total considered B region. Thus the wave functions, as plotted in Fig. 3, remain unchanged.

V. CONCLUSIONS

We studied an exciton in a type-II quantum disk of radius R and thickness d . For the confinement potential we took a hard wall of finite height, with the hole located in the barrier, which is only confined by the interaction with the electron, confined inside the dot. We calculated the exciton energy and wave function using the Hartree-Fock mesh method, which allows us to start without any knowledge of the single hole wave function. We limit ourselves to the study of a *model* system in which strain effects are neglected.

In the first part, we examined the case of an exciton in a single disk. First we investigated the exciton properties in the absence of a magnetic field. The calculation of the probability for the hole wave function to sit at the radial boundary tells us that we can distinguish two “regimes”: disklike systems with $d \ll 2R$, where the hole will prefer to sit above and below the quantum disk, and pillarlike systems with $d \gg 2R$, where the hole will be located at the radial boundary of the disk.

Applying a magnetic field along the z direction results in a different behavior for these two systems. For the disklike system, the hole is squeezed in the radial direction by the magnetic field, and the ground state of the system is the $l_h=0$ state for all values of B . For the pillarlike system, the magnetic field pushes the hole closer to the disk boundary, which forms a barrier for the hole. Therefore it will be energetically more favorable for the hole to jump to a higher angular momentum l_h state, as then the wave function is able to relax away from the radial boundary. With increasing magnetic field, we find successive l_h transitions.

The investigation of a system of two vertically coupled disks was done in order to compare its magnetic-field dependence with the pillarlike single-disk system. As was expected, we find again angular momentum transitions of the ground state. Moreover, a different feature appeared in this study, namely, a spontaneous symmetry breaking, induced by both the Coulomb interaction and the magnetic field. We found though that with increasing magnetic field, it is still preferable for the hole to jump to a higher angular momentum state. Investigation of a system of two vertically coupled truncated cones told us that also in this case angular momentum transitions occur, although the system is highly asymmetric.

A system of three vertically coupled disks was investigated in the third part of the paper. It was shown that the system with small interdot distance d_z behaves similarly to that of the single pillarlike disk. Again we found angular momentum transitions with increasing magnetic field. For a larger interdot distance, however, the hole wave function tends to sit between the disks. In this case, an increasing magnetic field does not lead to angular momentum transitions anymore, and the $l_h=0$ state remains the ground state. No spontaneous symmetry-broken states are found as the

ground state. This is similar to the single-disk system where symmetry-broken states occur only as excited states.

ACKNOWLEDGMENTS

K.L.J. is supported by the “Instituut voor de aanmoediging van Innovatie door Wetenschap en Technologie in Vlaanderen” (IWT-VI) and B.P. is a post-doctoral researcher with

the Flemish Science Foundation (FWO-VI). Discussions with M. Hayne, M. Tadić, and A. Matulis are gratefully acknowledged. Part of this work was supported by the FWO-VI, The Belgian Interuniversity Attraction Poles (IUAP), the Flemish Concerted Action (GOA) Programmes, the University of Antwerp, (VIS) and European Commission GROWTH program NANOMAT project, Contract No. GSRD-CT-2001-00545.

*Electronic address: karenj@uia.ua.ac.be

†Electronic address: bpartoen@uia.ua.ac.be

‡Electronic address: peeters@uia.ua.ac.be

¹For a review, see e.g., D. Bimberg, M. Grundmann, and N.N. Ledentsov, in *Quantum Dot Heterostructures* (Wiley, Chichester, 1999).

²A. Polimeni, S.T. Stoddart, M. Henini, L. Eaves, P.C. Main, K. Uchida, R.K. Hayden, and N. Miura, *Physica E (Amsterdam)* **2**, 662 (1998).

³L.R. Wilson, D.J. Mowbray, M.S. Skolnick, M. Morifuji, M.J. Steer, I.A. Larkin, and M. Hopkinson, *Phys. Rev. B* **57**, R2073 (1998).

⁴O. Stier, M. Grundmann, and D. Bimberg, *Phys. Rev. B* **59**, 5688 (1999).

⁵M. Brasken, M. Lindberg, D. Sundholm, and J. Olsen, *Phys. Rev. B* **61**, 7652 (2000).

⁶M. Bayer, A. Schmidt, A. Forchel, F. Faller, T.L. Reinecke, P.A. Knipp, A.A. Dremin, and V.D. Kulakovskii, *Phys. Rev. Lett.* **74**, 3439 (1995).

⁷J. Song and S.E. Ulloa, *Phys. Rev. B* **52**, 9015 (1995).

⁸K.L. Janssens, F.M. Peeters, and V.A. Schweigert, *Phys. Rev. B* **63**, 205311 (2001).

⁹M. Korkusinski and P. Hawrylak, *Phys. Rev. B* **63**, 195311 (2001).

¹⁰C.-K. Sun, G. Wang, J.E. Bowers, B. Brar, H.-R. Blank, H. Kroemer, and M. Pilkuhn, *Appl. Phys. Lett.* **68**, 1543 (1996).

¹¹L. Müller-Kirsch, R. Heitz, A. Schliwa, O. Stier, D. Bimberg, H. Kirmse, and W. Neumann, *Appl. Phys. Lett.* **78**, 1418 (2001).

¹²R. Heitz, N.N. Ledentsov, D. Bimberg, M.V. Maximov, A.Yu. Egorov, V.M. Ustinov, A.E. Zhukov, Zh.I. Alferov, G.E. Cirlin, I.P. Shoshnikov, N.D. Zakharov, P. Werner, and U. Gösele, *Appl. Phys. Lett.* **74**, 1701 (1999).

¹³S. Nomura, L. Samuelson, M.-E. Pistol, K. Uchida, N. Miura, T. Sugano, and Y. Aoyagi, *Appl. Phys. Lett.* **71**, 2316 (1997).

¹⁴M. Hayne, R. Provoost, M.K. Zundel, Y.M. Manz, K. Eberl, and V.V. Moshchalkov, *Phys. Rev. B* **62**, 10 324 (2000).

¹⁵M. Sugisaki, H.-W. Ren, K. Nishi, S. Sugou, T. Okuno, and Y. Masumoto, *Physica B* **256-258**, 169 (1998).

¹⁶F. Hatami, M. Grundmann, N.N. Ledentsov, F. Heinrichsdorff, R. Heitz, J. Böhrer, D. Bimberg, S.S. Ruvimov, P. Werner, V.M. Ustinov, P.S. Kop'ev, and Zh.I. Alferov, *Phys. Rev. B* **57**, 4635 (1998).

¹⁷C. Pryor, M.-E. Pistol, and L. Samuelson, *Phys. Rev. B* **56**, 10404 (1997).

¹⁸M. Tadic, F.M. Peeters, and K.L. Janssens, *Phys. Rev. B* **65**, 165333 (2002).

¹⁹S. Nomura, L. Samuelson, C. Pryor, M.-E. Pistol, M. Stopa, K. Uchida, N. Miura, T. Sugano, and Y. Aoyagi, *Phys. Rev. B* **58**, 6744 (1998).

²⁰K.L. Janssens, B. Partoens, and F.M. Peeters, *Phys. Rev. B* **64**, 155324 (2001).

²¹Ph. Lelong, K. Suzuki, G. Bastard, H. Sakaki, and Y. Arakawa, *Physica E (Amsterdam)* **7**, 393 (2000).

²²A.B. Kalameitsev, V.M. Kovalev, and A.O. Govorov, *Pis'ma Zh. Eksp. Teor. Fiz.* **68**, 634 (1998) [*JETP Lett.* **68**, 669 (1998)].

²³F.M. Peeters and V.A. Schweigert, *Phys. Rev. B* **53**, 1468 (1996).

²⁴S.E. Ulloa, A.O. Govorov, A.V. Kalameitsev, R. Warburton, and K. Karrai, *Physica E (Amsterdam)* **12**, 790 (2002).

²⁵A.O. Govorov, A.V. Kalameitsev, R. Warburton, K. Karrai, and S.E. Ulloa, *Physica E (Amsterdam)* **13**, 297 (2002).

²⁶We allowed for broken-symmetry solutions by manually pushing the electron single-particle wave function 0.1% more to the positive z direction with respect to the negative z direction in the first iteration step.